Applied Catalysis B: Environmental 321 (2023) 122035

Contents lists available at ScienceDirect

Applied Catalysis B: Environmental

journal homepage: www.elsevier.com/locate/apcatb

Chlorine anion stabilized Cu_2O/ZnO photocathode for selective CO_2 reduction to CH_4

Si-Tong Guo, Zi-Yuan Tang, Yu-Wei Du, Ting Liu, Ting Ouyang *, Zhao-Qing Liu *

School of Chemistry and Chemical Engineering/Institute of Clean Energy and Materials/Guangzhou Key Laboratory for Clean Energy and Materials, Guangzhou University, Guangzhou 510006, PR China

ARTICLE INFO

Keywords:
Cu_2O
Chlorine anion
CO_2 reduction
CH_4
Photoelectrocatalysis

ABSTRACT

Although Cu_2O-based material is one of the most promising catalysts, the deactivation of surface severely limits its selectivity and stablity. Here, we present a chlorine (Cl)-modified Cu_2O/ZnO heterostructure (CCZO) as photocathode with remarkable CH_4 faradaic efficiency (88.6 %) and durability (over 5 h). The Cl ions in CCZO serve as a passivator to stabilize Cu_2O against photo-corrosion. Stabilized Cu^+ active sites promote the hydrogenation of *CO intermediate, which provides a strong driving force for CO_2 reduction to CH_4. Calculation results indicate that for CCZO the hydrogenation of *CO trends to form *CHO (energy barrier of 0.220 eV) rather than CO (0.344 eV), further confirming the high selectivity of CCZO to CH_4. This work sheds insight on the catalytic mechanism of CCZO to modulate the energy barrier of intermediate *CO combined with H^+, providing a new idea to develop high selectivity and stable catalysts for CO_2 reduction.

1. Introduction

Catalytic reduction of CO_2 to fuels and chemicals coupled with alternative energy benefits to mitigate the rapid exhaustion of fossil resources and create a carbon-neutral cycle [1,2]. However, CO_2 conversion still suffers from the wide distribution of products with limited selectivity and the rapid deactivation of catalysts during operation [3,4]. Photoelectrocatalysis (PEC) is an ideal approach not only to utilize solar energy but also a method of energy storage by producing high value-added chemicals such as hydrocarbons or alcohols through CO_2 reduction processes [5–7]. Methane (CH_4) with impressive energy density ($\Delta H_C^\circ = 891$ kJ/mol), can be served as a hydrogen carrier being used in the chemical and energy industries [8–10]. However, the conversion of CO_2 to CH_4 sets off eight electrons and protons transfer, which needs to overcome high kinetic barrier [11–13]. Thus, developing highly efficient PEC catalysts for CO_2 reduction to CH_4 remains challenging.

Cu-based catalyst has been widely studied owing to its remarkable CO_2 reduction reaction (CO_2RR) performance, which is known to be the candidate that can convert CO_2 into hydrocarbons and alcohols [14–17]. In general, the adjacent Cu active sites over Cu-based surface facilitate C-C coupling, and increasing the distance between active sites can enhance the C_1 selectivity and suppress the C_2, which may be mainly attributed to the coverage and the spacing hindrance of *CO intermediates [18–20]. Meanwhile, the coverage of *CO is responsible for inhibiting hydrogen evolution reaction (HER) through the site blocking effects [21]. For CH_4, the hydrogenation of *CO to form *CHO is the rate-limiting step, and it also competes with the step of *CO to CO [22,23]. Experimental and theoretical studies proved that the adsorption energy of *CO is related to the oxidation state of Cu active sites. The reconstruction of Cu species induces changes in the adsorption of intermediates, which could be the cause of the decline in CH_4 selectivity [24,25]. Cu_2O is a p-type semiconductor with abundant natural resources, low toxicity, and appropriate band gaps for harvesting visible light, which has been used as a photocathode for CO_2 reduction [26–28]. And the controllable crystal planes and tunable active sites of Cu_2O provide a good platform to understand catalytic mechanisms [29,30]. Recently, the Cl-doping optimized band structure of Cu_2O to drive both CO_2 reduction and H_2O oxidation reactions, accelerating the separation of photoinduced electron-hole pairs [31]. After photocatalytic reaction using visible-light illumination, the yields of CO and CH_4 for Cl-doped Cu_2O were 1.74 μmol cm^{-2} and 0.39 μmol cm^{-2}, respectively, which increased to 7 and 15 times than that of pure Cu_2O. In addition, the Si/ZnO/Cu_2O p-n-p heterojunction was applied for photoelectrocatalytic CO_2 reduction [32]. Due to the existence of a potential well by growing n-type ZnO between Cu_2O and Si, the selectivity of CO_2 reduction for Si/ZnO/Cu_2O is turned from CO or formate to ethanol with

* Corresponding authors.
E-mail addresses: ouyt@gzhu.edu.cn (T. Ouyang), lzqgzu@gzhu.edu.cn (Z.-Q. Liu).

https://doi.org/10.1016/j.apcatb.2022.122035
Received 22 August 2022; Received in revised form 26 September 2022; Accepted 30 September 2022
Available online 1 October 2022

FE over 60 %. Although the selectivity of products has been reported in some photoelectrochemical CO_2 reduction studies, the detailed mechanism for foreign anion-modified Cu_2O heterojunctions is still unclear.

Herein, we propose a facile two-step electrodeposition method to synthesize Cl-modified Cu_2O/ZnO as photocathode. The constructed Cu_2O/ZnO heterojunction effectively improves the carrier separation The Cl-ions act as the passivator for stabilizing the Cu^+ active sites over catalysts surface, which contributes to retain the outperformance of CH_4 selectivity (88.6 % at − 0.3 V vs. RHE) and durability (over 5 h). Theoretical calculation shows that the CCZO catalyst decreases the energy barrier of key step from *CO to *CHO, suggesting that the hydrogenation of *CO is more energy favorable than the CO desorption. This work provides a new insight into the mechanism of anion modification and benefits the rational design of highly efficient photocathode for CO_2 reduction to CH_4.

2. Experimental section

2.1. Synthesis of ZnO nanorod arrays

The ZnO nanorods (denoted as ZnO NRAs) grown on fluorine-doped tin dioxide conductive glass (FTO) were prepared by electrodeposition method in three electrode solution system. The solution of ZnO electrodeposition contained 0.02 M $Zn(NO_3)_2{\cdot}6\mathbf{H}_2O$, 0.01 M HMT and 0.01 M NH_4AC. Carbon rod was used as counter electrode and the FTO was used as working electrode. The ZnO NRAs grown on FTO under the condition of constant current of − 2 mA and 90 ℃ for 50 min through the galvanostatic method [33,34].

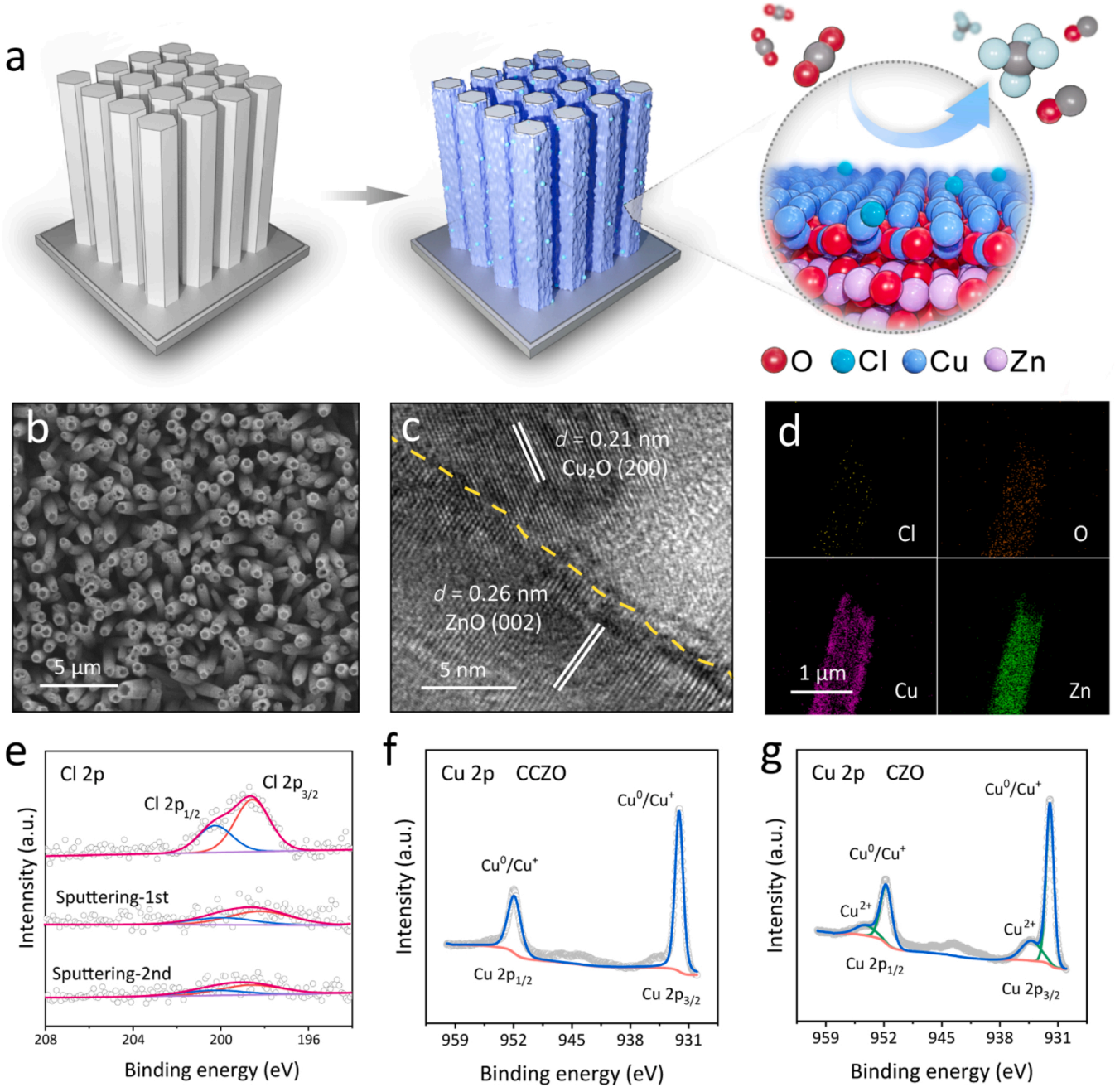

Fig. 1. a) Schematic illustration for the synthesis of CCZO, b) Top view SEM images, c) HRTEM image, d) corresponding EDS elemental mapping images, and e) Cl 2p XPS spectra with argon-ions sputtering for CCZO. Cu 2p XPS spectra for f) CCZO and g) CZO.

2.2. Synthesis of CCZO and CZO

The Cu_2O/ZnO nanorod arrays (denoted as CZO) were synthesized by an electrodeposition process according to the previous reports with minor modifications. Electrodeposition was conducted in a three-electrode system, where the ZnO/FTO was used as the working electrode, Pt as the counter electrode, and Ag/AgCl electrode as the reference electrode. To synthesize the Cl-modified Cu_2O/ZnO (denoted as

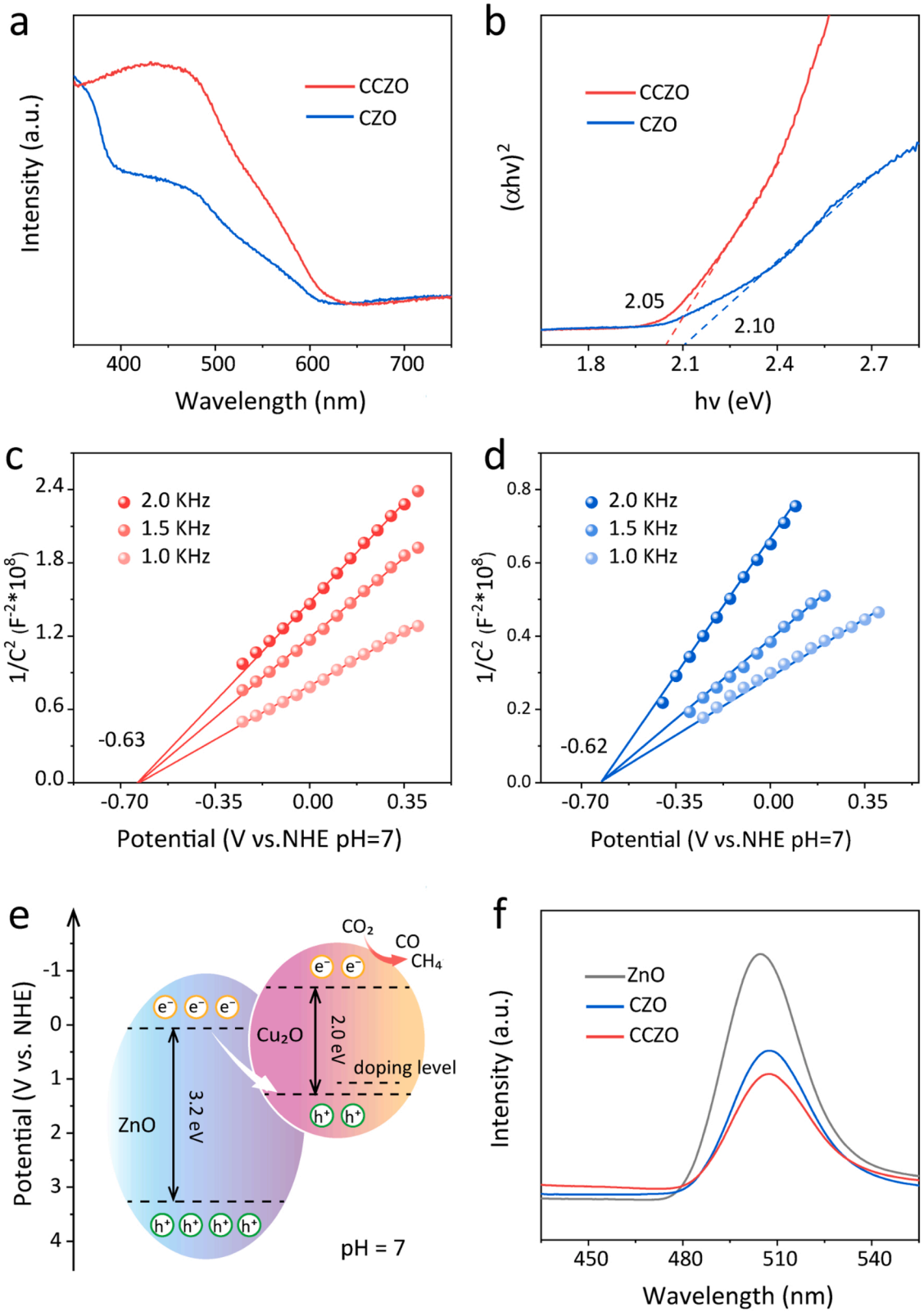

Fig. 2. a) UV–vis and b) Tauc plot for CCZO and CZO. Mott-Schottky plots for c) CCZO, and d) CZO. e) Band structure alignment of CCZO. f) PL spectra for CCZO, CZO and ZnO.

CCZO), the solution for Cu_2O electrodeposition contained 0.05 M $CuCl_2$ and 1.67 M lactic acid. The pH was adjusted to 7.5 by the addition of 4 M NaOH solution. The deposition system was kept at a temperature of 60 °C, and a voltage of − 0.2 V vs. Ag/AgCl for 40 min. The CZO was prepared using the same method with the addition of $CuSO_4$ as the anion source [31].

3. Result and discussion

3.1. Morphology and structure properties

The CCZO was synthesized via a two-step electrodeposition method as illustrated in Fig. 1a. First, the ZnO precursor was fabricated on fluorine-doped tin dioxide conductive glass (FTO), followed by electrodeposition of Cu_2O with $CuCl_2$ as Cl source. The control sample was prepared with $CuSO_4$ as the anion source by a similar method, which is denoted as CZO. X-ray diffraction (XRD) patterns was carried out to characterize the crystal structure. The diffraction peaks are attributed to ZnO and Cu_2O without detectable impurities phases, confirming the formation of Cu_2O and ZnO (Fig. S1). The scanning electron microscopy (SEM) and transmission electron microscopy (TEM) images present that ZnO has a hexagonal prism-shaped morphology with smooth surface (Fig. S2) and Cu_2O nanoparticles are uniformly decorated on it (Fig. 1b). After secondary electrodeposition, CCZO well preserves the 1D morphology and increased surface roughness which is favorable to provide high surface area and active sites (Fig. S3) [35]. High-resolution transmission electron microscopy (HRTEM) image shows that the lattice fringes with spacings of 0.21 nm and 0.26 nm, which can be assigned to the facets of Cu_2O (200) and ZnO (002), respectively (Figs. 1c and S4). Energy-dispersive X-ray spectroscopy (EDS) mapping further confirms the presence of Cl, Cu, Zn, and O elements in the composite (Figs. 1d and S5). X-ray photoelectron spectroscopy (XPS) was used to investigate the chemical composition and valence states (Fig. S6). The Cl 2p spectrum for CCZO shows a peak at 198 eV, which can be assigned to Cl^- (Fig. 1e). XPS spectra assisted with argon-ions sputtering (20 nm each time) results in a significant decrease in the signal of Cl peak, suggesting that Cl species are mainly located at the surface and

partly doped into the lattice of Cu_2O. In the Cu 2p spectra, two main peaks can be assigned to Cu^0/Cu^+ at 932.0 eV and 951.9 eV (Fig. 1f). Besides that, compared with CCZO, an obvious increase in the signal of Cu^{2+} for CZO can be observed at 934.7 eV and 954.4 eV (Fig. 1g) [36]. The above results suggest that the modification of Cl ions stabilizes the Cu^+ active sites.

3.2. Photochemical properties

The optical absorption properties and bandgap energies were investigated by UV–vis diffuse reflectance spectroscopy (DRS). The strong absorption peaks range from 420 nm to 480 nm are observed in CCZO and CZO (Fig. 2a). Corresponding bandgap energies calculated by Tauc plot show that CCZO and CZO are 2.05 eV and 2.10 eV, respectively, demonstrating that they can both be excited by visible light to generate electron-hole pairs (Fig. 2b) [37]. It is possible that the doping of Cl leads to the formation of some localized states, resulting in a narrow bandgap. The type of semiconductor was investigated by the Motte-Schottky plots. Results reveal that ZnO is n-type semiconductor and the Cu_2O/ZnO composite with p-n junction (Fig. S7). Besides that, the derived flat-band potentials for CCZO and CZO are determined to be − 0.63 V and − 0.62 V vs. NHE (Fig. 2c–d), demonstrating that the synthesized catalysts have appropriate redox potential for CO_2RR (Table S1) [38]. Furthermore, the energy band structure of ZnO was further characterized by X-ray photoelectron spectroscopy (UPS). The VB and CB are 3.24 V and 0.04 V vs. NHE, respectively (Figs. S8 and S9). According to the previous reports, the VB and CB of Cl-modified Cu_2O is 1.12 V and − 0.88 V vs. NHE. Based above results, the band structure alignment of CCZO is proposed in Fig. 2e. The photogenerated carriers proceed a Z-shape pathway that facilitates the efficient transfer of electrons to catalyst surface for the reduction reaction [39,40]. The separation-recombination rate of photogenerated carriers was further estimated by photoluminescence (PL) characterization. CCZO and CZO exhibit a remarkable fluorescence quenching compared to ZnO, indicating the lower electron-hole recombination rate (Fig. 2f) [41].

3.3. PEC CO_2 reduction performance

Upon tracing the optical properties, the PEC performance of CCZO and CZO was investigated in three-electrode quartz system with Pt plate as counter electrodes and Ag/AgCl as the reference electrode. Linear sweep voltammetry (LSV) for CCZO was tested in the CO_2 and N_2-saturated 0.1 M $KHCO_3$ solutions. The current density significantly increases with visible light irradiation under CO_2 and N_2 atmosphere (Fig. 3a). Meanwhile, a larger current density can be obtained in the CO_2 atmosphere, indicating the occurrence of CO_2 reduction on catalyst surface. We further compared the current density of LSV curves for CCZO and CZO in CO_2 atmosphere with visible light irradiation. The cathode current density of CCZO is higher than that of CZO, suggesting that the PEC performance of CCZO is better than that of CZO (Fig. 3b). After 30 min of each electrolytic reaction, the gas- and liquid-phase products from the cathode compartment were analyzed by gas chromatography (GC) and nuclear magnetic resonance (NMR), and further calculated their FEs. With the applied potential ranges from − 0.3 V to − 0.6 V vs. RHE, CH_4 was detected as the primary product with minor CO and H_2, and no liquid product was produced (Figs. S10 and S11). As shown in Fig. 3c–d, CCZO keeps high FEs toward CH_4 (>65 %) with FEs of CO and H_2 lower than 20 %. The production of CH_4 for CCZO increase form 0.61 μmol to 1.04 μmol, and corresponding FEs are from 88.6 % to 68.6 % with the applied potential from − 0.3 to − 0.6 V vs. RHE. In comparison, the production of CH_4 for CZO.

decreases from 0.73 μmol to 0.40 μmol, while that of H_2 is 0.78 μmol with the applied potential increased from − 0.3 to − 0.6 V vs. RHE (Figs. S12 and S13). Compared to CZO, CCZO demonstrates high CH_4 selectivity with strong H_2 and CO suppression especially at a higher potential. The ratio of FE_{CH4} to FE_{H2} for CCZO is 8.0 (at − 0.6 V vs. RHE), whereas that for CZO is 2.7. These results imply that Cl ions attribute to promote CO_2RR prosses instead of HER. A series of experiments were executed to verify the source of products. When CO_2 reactant is replaced by N_2, a small amount of H_2 but no CO_2 reduction products can be detectable (Fig. S14). ^{13}C labeling experiment was further carried out to provide the direct proof of carbon source, in which the peak at $m/z = 17$ ($^{13}CH_4$) can be observed, demonstrating that the CH_4 is indeed derived from the CO_2 reduction (Fig. 3e) [42]. In addition, the chronoamperometry I-t curve was carried out to assess the stability. CCZO exhibits a nearly stable photocurrent density at − 0.4 V vs. RHE for 5 h of continuous CO_2 reduction reaction (Fig. 3f). By contrast, unstable current density for CZO is observed under continuous or intermittent illumination (Fig. S15). Spectroscopic characterization is further conducted to elucidate the possible phase change after stability measurements. XRD results indicate that the crystal phase remains unchanged for CCZO but the emergence of new phase for CZO (Fig. S16). XPS results confirm that the chemical states of Cl on surfaces did not undergo significant changes (Fig. S17). In situ XPS spectra were carried out to investigate the photo-stability of catalyst under light irradiation. As shown in Fig. 4a–b, the peaks attributed to Cu and Cl species shows no significant change upon light irradiation. These results reveal that CCZO exhibits enhanced photostability and Cl-modified improve the durability of Cu_2O.

3.4. Mechanism analysis

To further reveal the origin of the different performances for CCZO and CZO, the electrochemically active surface area (ECSA) was measured to investigate the of catalysts by the double-layer capacitance

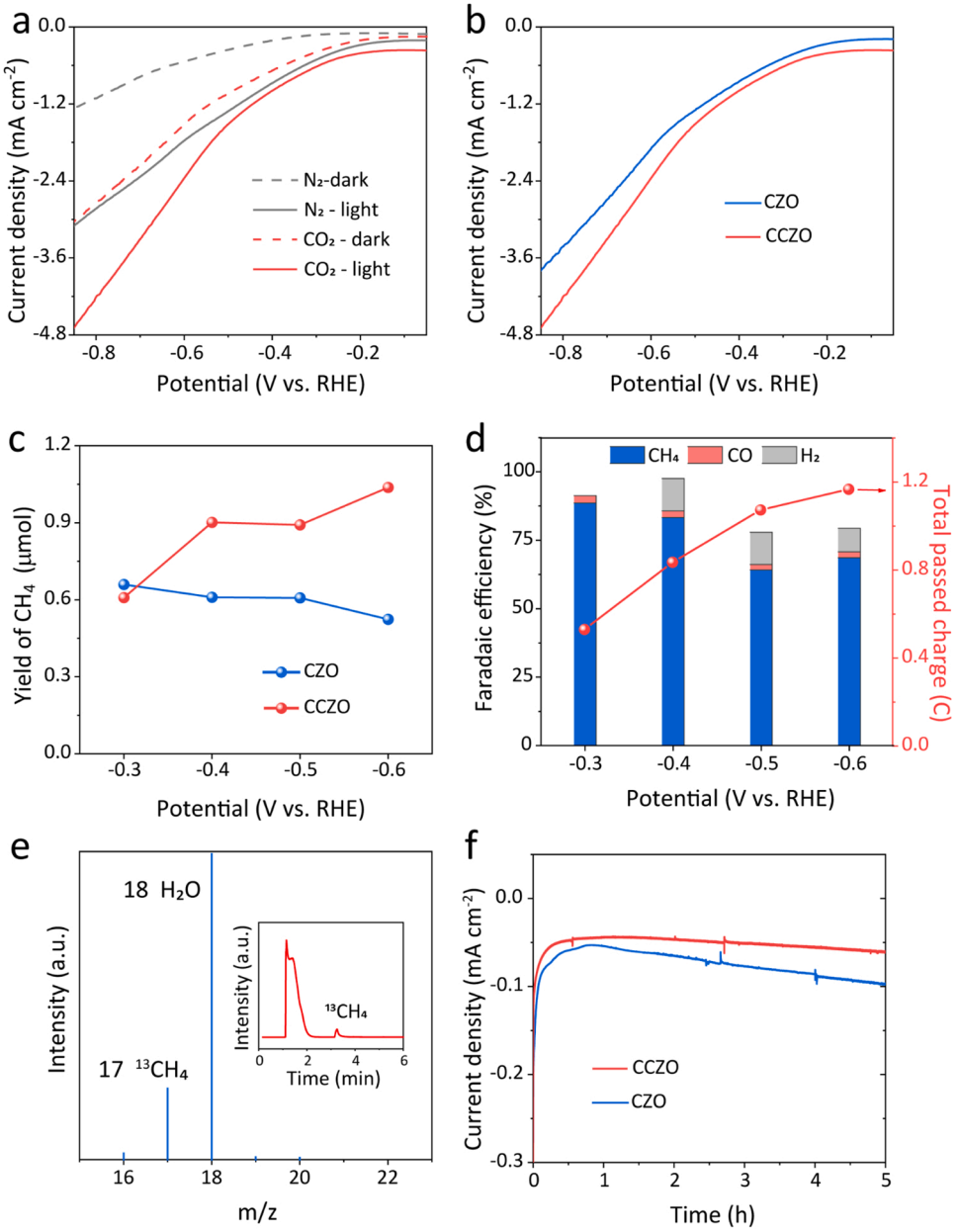

Fig. 3. PEC activity for CO_2 reduction in 0.1 M $KHCO_3$ electrolyte. a) LSV curves under: N_2 dark/light, CO_2 dark/light for CCZO. b) LSV curves under CO_2 with visible light irradiation and c) CH_4 Yields for CCZO and CZO. d) FEs and total passed charge at different applied potentials for CCZO. e) GC-MS analysis of carbon products in $^{13}CO_2$ reduction using CCZO as photocathode. f) Stability test for CCZO and CZO.

method (Figs. 4c and S18). The ECSA value of CCZO (0.59 mF cm^{-2}) is 3.3-flod to that of CZO (0.18 mF cm^{-2}), suggesting that the electrochemical surface areas significantly increase after modification of Cl ions. Electrochemical impedance spectroscopy (EIS) results reveal that CCZO has a lower charge-transfer resistance and quicker electron transfer (Fig. 4d). It is known that *CO is an important intermediate in the conversion of CO_2 to CH_4 [43–45]. The key step in the formation CH_4 is the hydrogenation of the adsorbed CO to form CHO_{ads}. The above process depends on pH since the rate-determining step involves the transfer of H^+- e^- [46,47]. Thus, we adjust the electrolyte to change the local pH value to test the CH_4 selectivity of CCZO. Local pH at the electrode/electrolyte interface is an important factor affecting the selectivity of the CO_2RR products [48]. Smith et al. showed that for the Cu nanowire array electrodes in high pH electrolytes (0.1 M $KClO_4$ without buffer ability) favor formation of C_2H_4 with suppressed H_2 evolution, while in the low pH electrolytes (0.1 M K_2HPO_4 with strong buffer ability) favors H_2 evolution [49]. To understand the distribution of products as a function of local pH for CCZO, electrolytes of 0.1 M K_2HPO_4, $KHCO_3$, and K_2SO_4 with different buffer ability (K_2SO_4 < $KHCO_3$ < K_2HPO_4) were chosen to regulate the local pH (Fig. 4e). In the three electrolytes, K_2SO_4 with the worst buffer ability and highest local pH, which is not conducive for H_2O activation; while the K_2HPO_4 with the best buffer ability and smallest local pH, which is useful for H_2O activation. For CCZO with 0.1.

M K_2SO_4 as electrolyte at 0.4 V vs. RHE, the formation of CH_4 (FE 84.3 %), CO (FE 3.5 %) is observed, while with $KHCO_3$ as electrolyte, the formation of CH_4 (FE 83.7 %), CO (FE 2.4 %), H_2 (FE 11.9 %) is observed; With 0.1 M K_2HPO_4 as electrolyte, the formation of CH_4 (FE 38.6 %), CO (FE 1.0 %), H_2 (FE 20.0 %) is observed (Fig. 4f). The above findings indicate that the selectivity for CO_2RR to CH_4 can be tuned on CCZO by varying the local pH. And the enhanced selectivity for H_2 with suppressed CO_2 reduction is observed in K_2HPO_4, suggesting that the

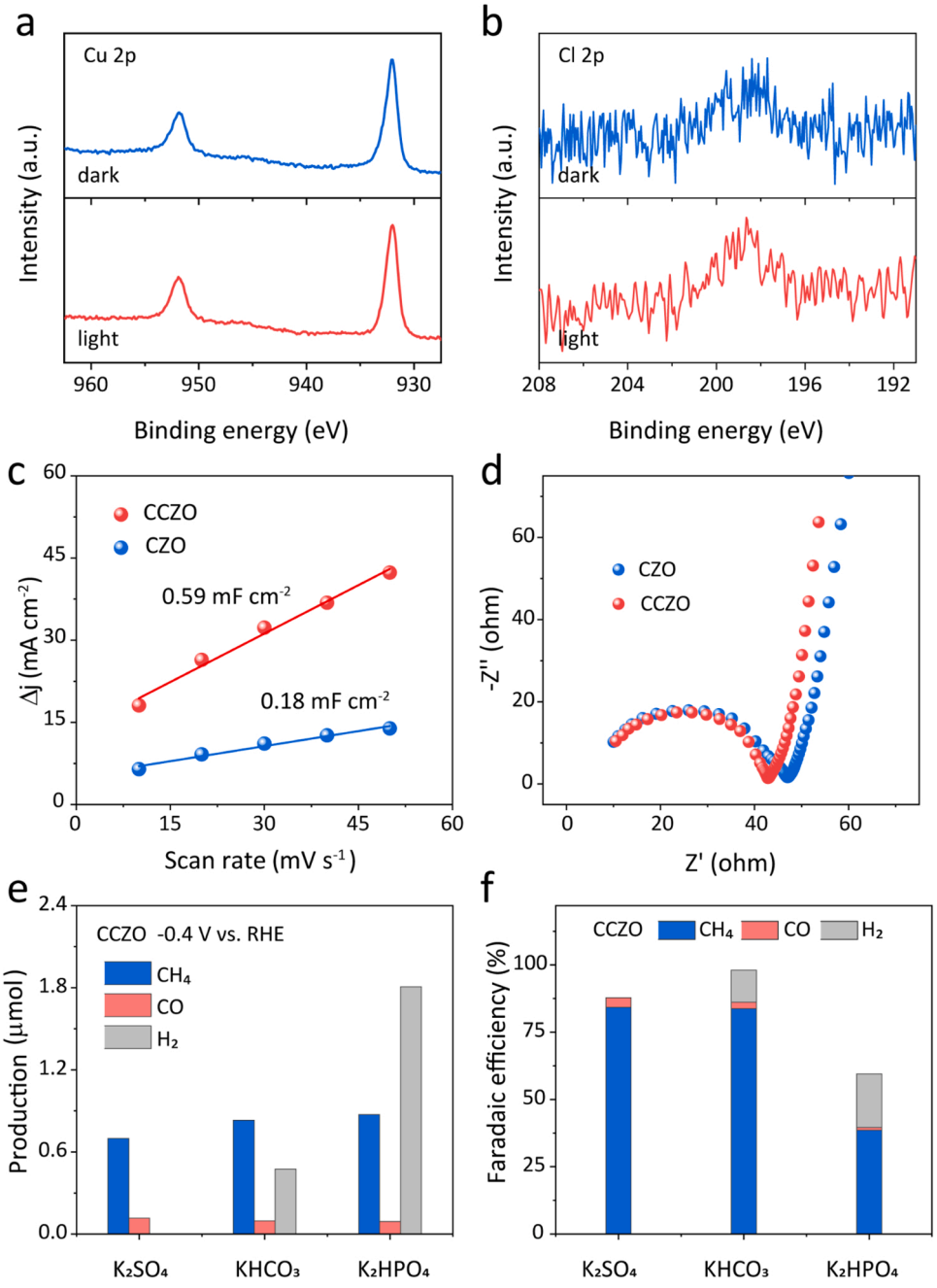

Fig. 4. In situ high-resolution a) Cu 2p and b) Cl 2p XPS spectra for CCZO in the dark and under light irradiation. c) ECSA and d) EIS for CCZO and CZO. e, f) Effect of electrolytes or pH on performances for CO_2 reduction over CCZO.

local pH plays a significant role for the CCZO in CO_2 reduction, which suggested that this pathway is limited by a later H^+-e^- transfer [50]. This conclusion agrees well with Peterson's observations: "the key step in the formation of the hydrocarbons CH_4 is the hydrogenation of the adsorbed CO to form CHO_{ads}". Meanwhile, CH_4 production exhibits a limiting impact on local pH, even though HER becomes dominant at lower local pH. The results reveal that Cu^+ active sites promote the hydrogenation of *CO over H_2 evolution, which could be the main mechanism by which CCZO maintains a high FE of CO_2 reduction product. Density functional theory (DFT) calculations were performed to further understand the CO_2-to-CH_4 mechanism and the high selectivity on CCZO. Based on the results of HRTEM, we have built Cl-modified Cu_2O (220)/ZnO (100) interfaces as research model and constructed the reaction pathways of CO_2-to-CO and CO_2-to-CH_4 according to the pathway proposed by Peterson et. al (Fig. 5) [51]. As depicted in Fig. 5a and b, the reaction pathway of CO_2-to-CO is: CO_2 → *CO_2 → *COOH → *CO →CO, and the reaction pathway of CO_2-to-CH_4 is: CO_2 → *CO_2 → *COOH → *CO → *CHO → *CH_2O → *CH_3O → CH_4. It should be inferred that both CO and CH_4 evolution pathway undergo the intermediate of *CO. The energy barrier for the hydrogenation of *CO to *CHO is 0.220 eV, whereas that for CO directly desorption is 0.344 eV, suggesting that the CH_4 selectivity is observed by rising the energy barrier for the competing step of CO generation. DTF calculated results demonstrate the CO_2 reduction over CCZO surface prefers to proceed the CH_4 pathway rather than the CO pathway, which confirmed CCZO possesses high selectivity of CH_4.

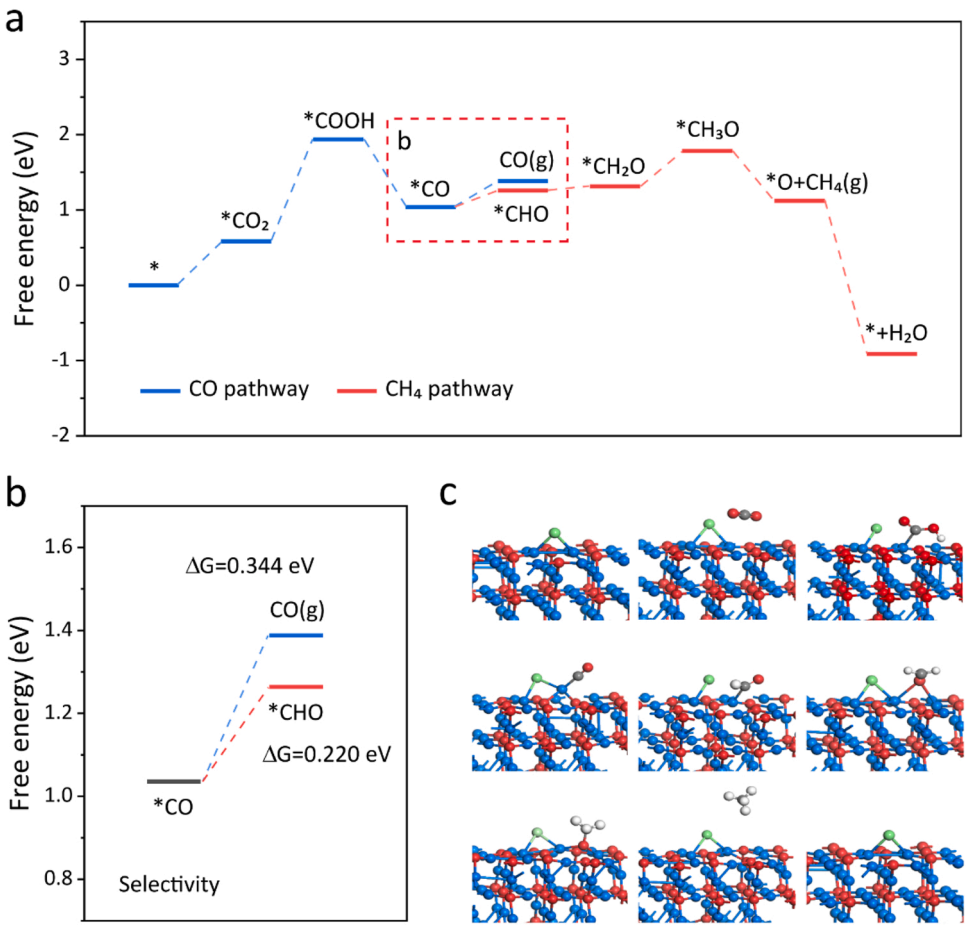

Fig. 5. a, b) Reaction energy diagram for CH_4 and CO pathway for CCZO. c) The optimized structures for main reaction intermediates. The green, blue, gray, red and white balls represent Cl, Cu, C, O and H elements, respectively.

4. Conclusion

In summary, we demonstrate a facile method to stabilize Cu_2O by introducing Cl ions. And the anion-modified Cu_2O/ZnO heterostructure shows remarkable performance for PEC CO_2 to CH_4. High CH_4 selectivity with the strong suppression of H_2 and CO and its link with the functional mechanism of Cl ions were verified by experimental and theoretical methods. Compared to the pristine Cu_2O/ZnO, the durability of Cl-assisted Cu_2O is obtained over the same period by protecting the activity of Cu^+ site. Simultaneously, kinetic experiments and DFT calculations prove that the presence of Cl ions suppresses HER and boosts the hydrogenation of *CO to form *CHO (energy barrier of 0.220 eV) rather than CO (0.344 eV), resulting in CCZO possesses high selectivity of 88.6% for CH_4 and remarkable durability. This work provides a facile strategy for the design of efficient photocathodes for CO_2 reduction to CH_4 and broadens the understanding of anion modification being used in the PEC systems.

CRediT authorship contribution statement

T. Ouyang and **Prof. Z-Q. Liu** conceived and designed the project, **S. T. Guo, Z. Y. Tang, Y. W. Du**, and **T. Liu** performed the experiments and carried out the DFT calculations, **S. T. Guo, T. Ouyang** and **Z-Q. Liu** analyzed the data, wrote and revised the article.

Declaration of Competing Interest

The authors declare that they have no known competing financial interests or personal relationships that could have appeared to influence the work reported in this paper.

Data availability

Data will be made available on request.

Acknowledgements

This work was financially supported by National Natural Science Foundation of China (Grant No. 21875048, 21905063 and 22278094), Outstanding Youth Project of Guangdong Natural Science Foundation (No. 2020B1515020028), Guangdong Natural Science Foundation (Grant No. 2021A1515010066), University Innovation Team Scientific Research Project of Guangzhou Education Bureau (No. 202235246).

Appendix A. Supporting information

Supplementary data associated with this article can be found in the online version at doi:10.1016/j.apcatb.2022.122035.

References

[1] M.B. Ross, P. De Luna, Y. Li, C.-T. Dinh, D. Kim, P. Yang, E.H. Sargent, Designing materials for electrochemical carbon dioxide recycling, Nat. Catal. 2 (2019) 648–658, https://doi.org/10.1038/s41929-019-0306-7.
[2] X. Meng, G. Zuo, P. Zong, H. Pang, J. Ren, X. Zeng, S. Liu, Y. Shen, W. Zhou, J. Ye, A rapidly room-temperature-synthesized Cd/ZnS:Cu nanocrystal photocatalyst for highly efficient solar-light-powered CO_2 reduction, Appl. Catal. B Environ. 237 (2018) 68, https://doi.org/10.1016/j.apcatb.2018.05.066.
[3] S. Nitopi, E. Bertheussen, S.B. Scott, X. Liu, A.K. Engstfeld, S. Horch, B. Seger, I.E. L. Stephens, K. Chan, C. Hahn, J.K. Nørskov, T.F. Jaramillo, I. Chorkendorff,

Progress and perspectives of electrochemical CO_2 reduction on copper in aqueous electrolyte, Chem. Rev. 119 (2019) 7610–7672, https://doi.org/10.1021/acs.chemrev.8b00705.
[4] A. Vasileff, Y. Zhu, X. Zhi, Y. Zhao, L. Ge, H.M. Chen, Y. Zheng, S.-Z. Qiao, Electrochemical reduction of CO_2 to ethane through stabilization of an ethoxy intermediate, Angew. Chem. Int. Ed. 59 (2020) 19649–19653, https://doi.org/10.1002/anie.202004846.
[5] H. Wu, H.L. Tan, C.Y. Toe, J. Scott, L. Wang, R. Amal, Y.H. Ng, Photocatalytic and photoelectrochemical systems: similarities and differences, Adv. Mater. 32 (2020), 1904717, https://doi.org/10.1002/adma.201904717.
[6] Y. Zhou, F. Che, M. Liu, C. Zou, Z. Liang, P. De Luna, H. Yuan, J. Li, Z. Wang, H. Xie, H. Li, P. Chen, E. Bladt, R. Quintero-Bermudez, T.-K. Sham, S. Bals, J. Hofkens, D. Sinton, G. Chen, E.H. Sargent, Dopant-induced electron localization drives CO_2 reduction to C_2 hydrocarbons, Nat. Chem. 10 (2018) 974–980, https://doi.org/10.1038/s41557-018-0092-x.
[7] A.U. Pawar, U. Pal, J.Y. Zheng, C.W. Kim, Y.S. Kang, Thermodynamically controlled photo-electrochemical CO_2 reduction at Cu/rGO/PVP/Nafion multi-layered dark cathode for selective production of formaldehyde and acetaldehyde, Appl. Catal. B Environ. 303 (2022), 120921, https://doi.org/10.1016/j.apcatb.2021.120921.
[8] J. Shen, R. Kortlever, R. Kas, Y.Y. Birdja, O. Diaz-Morales, Y. Kwon, I. Ledezma-Yanez, K.J.P. Schouten, G. Mul, M.T.M. Koper, Electrocatalytic reduction of carbon dioxide to carbon monoxide and methane at an immobilized cobalt protoporphyrin, Nat. Commun. 6 (2015) 8177, https://doi.org/10.1038/ncomms9177.
[9] P. Lianos, Review of recent trends in photoelectrocatalytic conversion of solar energy to electricity and hydrogen, Appl. Catal. B Environ. 210 (2017) 235, https://doi.org/10.1016/j.apcatb.2017.03.067.
[10] Y. Dou, A. Zhou, Y. Yao, S.Y. Lim, J.-R. Li, W. Zhang, Suppressing hydrogen evolution for high selective CO_2 reduction through surface-reconstructed heterojunction photocatalyst, Appl. Catal. B Environ. 286 (2021), 119876, https://doi.org/10.1016/j.apcatb.2021.119876.
[11] B. Zhou, P. Ou, N. Pant, S. Cheng, S. Vanka, S. Chu, T. Rashid Roksana, G. Botton, J. Song, Z. Mi, Highly efficient binary copper−iron catalyst for photoelectrochemical carbon dioxide reduction toward methane, Proc. Natl. Acad. Sci. USA 117 (2020) 1330–1338, https://doi.org/10.1073/pnas.1911159117.
[12] Y. Wang, Z. Chen, P. Han, Y. Du, Z. Gu, X. Xu, G. Zheng, Single-atomic cu with multiple oxygen vacancies on ceria for electrocatalytic CO_2 reduction to CH_4, ACS Catal. 8 (2018) 7113–7119, https://doi.org/10.1021/acscatal.8b01014.
[13] D. Xu, B. Cheng, W. Wang, C. Jiang, J. Yu, Ag_2CrO_4/g-C_3N_4/graphene oxide ternary nanocomposite Z-scheme photocatalyst with enhanced CO_2 reduction activity, Appl. Catal. B Environ. 231 (2018) 368, https://doi.org/10.1016/j.apcatb.2018.03.036.
[14] Z. Weng, X. Zhang, Y. Wu, S. Huo, J. Jiang, W. Liu, G. He, Y. Liang, H. Wang, Self-cleaning catalyst electrodes for stabilized CO_2 reduction to hydrocarbons, Angew. Chem. Int. Ed. 56 (2017) 13135–13139, https://doi.org/10.1002/anie.201707478.
[15] Y. Zheng, A. Vasileff, X. Zhou, Y. Jiao, M. Jaroniec, S.-Z. Qiao, Understanding the roadmap for electrochemical reduction of CO_2 to multi-carbon oxygenates and hydrocarbons on copper-based catalysts, J. Am. Chem. Soc. 141 (2019) 7646–7659, https://doi.org/10.1021/jacs.9b02124.
[16] J. He, K.E. Dettelbach, D.A. Salvatore, T. Li, C.P. Berlinguette, High-throughput synthesis of mixed-metal electrocatalysts for CO_2 reduction, Angew. Chem. Int. Ed. 56 (2017) 6068–6072, https://doi.org/10.1002/anie.201612038.
[17] P. Li, J. Bi, J. Liu, Q. Zhu, C. Chen, X. Sun, J. Zhang, B. Han, In situ dual doping for constructing efficient CO_2-to-methanol electrocatalysts, Nat. Commun. 13 (2022) 1965, https://doi.org/10.1038/s41467-022-29698-3.
[18] A. Guan, Q. Wang, Y. Ji, S. Li, C. Yang, L. Qian, L. Zhang, L. Wu, G. Zheng, Steric effect induces CO electroreduction to CH_4 on Cu–Au alloys, J. Mater. Chem. A 9 (2021) 21779–21784, https://doi.org/10.1039/D1TA06162C.
[19] A. Guan, Z. Chen, Y. Quan, C. Peng, Z. Wang, T.-K. Sham, C. Yang, Y. Ji, L. Qian, X. Xu, G. Zheng, Boosting CO_2 electroreduction to CH_4 via tuning neighboring single-copper sites, ACS Energy Lett. 5 (2020) 1044–1053, https://doi.org/10.1021/acsenergylett.0c00018.
[20] W. Ma, X. He, W. Wang, S. Xie, Q. Zhang, Y. Wang, Electrocatalytic reduction of CO_2 and CO to multi-carbon compounds over Cu-based catalysts, Chem. Soc. Rev. 50 (2021) 12897–12914, https://doi.org/10.1039/D1CS00535A.
[21] H. Ooka, M.C. Figueiredo, M.T.M. Koper, Competition between hydrogen evolution and carbon dioxide reduction on copper electrodes in mildly acidic media, Langmuir 33 (2017) 9307–9313, https://doi.org/10.1021/acs.langmuir.7b00696.
[22] A. Bagger, W. Ju, A.S. Varela, P. Strasser, J. Rossmeisl, Electrochemical CO_2 reduction: a classification problem, ChemPhysChem 18 (2017) 3266–3273, https://doi.org/10.1002/cphc.201700736.
[23] B. Li, L. Sun, J. Bian, N. Sun, J. Sun, L. Chen, Z. Li, L. Jing, Controlled synthesis of novel Z-scheme iron phthalocyanine/porous WO_3 nanocomposites as efficient photocatalysts for CO_2 reduction, Appl. Catal. B Environ. 270 (2020), 118849, https://doi.org/10.1016/j.apcatb.2020.118849.
[24] X. Yuan, S. Chen, D. Cheng, L. Li, W. Zhu, D. Zhong, Z.-J. Zhao, J. Li, T. Wang, J. Gong, Controllable Cu^0-Cu^+ sites for electrocatalytic reduction of carbon dioxide, Angew. Chem. Int. Ed. 60 (2021) 15344–15347, https://doi.org/10.1002/anie.202105118.
[25] A.A. Peterson, J.K. Nørskov, Activity descriptors for CO_2 electroreduction to methane on transition-metal catalysts, J. Phys. Chem. Lett. 3 (2012) 251–258, https://doi.org/10.1021/jz201461p.
[26] X. Deng, R. Li, S. Wu, L. Wang, J. Hu, J. Ma, W. Jiang, N. Zhang, X. Zheng, C. Gao, L. Wang, Q. Zhang, J. Zhu, Y. Xiong, Metal–organic framework coating enhances the performance of Cu_2O in photoelectrochemical CO_2 reduction, J. Am. Chem. Soc. 141 (2019) 10924–10929, https://doi.org/10.1021/jacs.9b06239.
[27] Y. Zhang, D. Pan, Y. Tao, H. Shang, D. Zhang, G. Li, H. Li, Photoelectrocatalytic reduction of CO_2 to syngas via SnO_x-enhanced Cu_2O nanowires photocathodes, Adv. Funct. Mater. 32 (2022), 2109600, https://doi.org/10.1002/adfm.202109600.
[28] F. Zhang, Y.-H. Li, M.-Y. Qi, Z.-R. Tang, Y.-J. Xu, Boosting the activity and stability of Ag-Cu_2O/ZnO nanorods for photocatalytic CO_2 reduction, Appl. Catal. B Environ. 268 (2020), 118380, https://doi.org/10.1016/j.apcatb.2019.118380.
[29] B. Deng, M. Huang, K. Li, X. Zhao, Q. Geng, S. Chen, H. Xie, Xa Dong, H. Wang, F. Dong, The crystal plane is not the key factor for CO_2-to-methane electrosynthesis on reconstructed Cu_2O microparticles, Angew. Chem. Int. Ed. 61 (2022), e202114080, https://doi.org/10.1002/anie.202114080.
[30] W. Shi, X. Guo, C. Cui, K. Jiang, Z. Li, L. Qu, J.-C. Wang, Controllable synthesis of Cu_2O decorated WO_3 nanosheets with dominant (0 0 1) facets for photocatalytic CO_2 reduction under visible-light irradiation, Appl. Catal. B Environ. 243 (2019) 236, https://doi.org/10.1016/j.apcatb.2018.09.076.
[31] L. Yu, X. Ba, M. Qiu, Y. Li, L. Shuai, W. Zhang, Z. Ren, Y. Yu, Visible-light driven CO_2 reduction coupled with water oxidation on Cl-doped Cu_2O nanorods, Nano Energy 60 (2019) 576–582, https://doi.org/10.1016/j.nanoen.2019.03.083.
[32] M. Kan, C. Yang, Q. Wang, Q. Zhang, Y. Yan, K. Liu, A. Guan, G. Zheng, Defect-assisted electron tunneling for photoelectrochemical CO_2 reduction to ethanol at low overpotentials, Adv. Energy Mater. 12 (2022), 2201134, https://doi.org/10.1002/aenm.202201134.
[33] S. Huang, T. Ouyang, B.-F. Zheng, M. Dan, Z.-Q. Liu, Enhanced photoelectrocatalytic activities for CH_3OH-to-HCHO conversion on Fe_2O_3/MoO_3: Fe-O-Mo covalency dominates the intrinsic activity, Angew. Chem. Int. Ed. 60 (2021) 9546–9552, https://doi.org/10.1002/anie.202101058.
[34] R.B. Wei, P.Y. Kuang, H. Cheng, Y.B. Chen, J.Y. Long, M.Y. Zhang, Z.Q. Liu, Plasmon-enhanced photoelectrochemical water splitting on gold nanoparticle decorated ZnO/CdS nanotube arrays, ACS Sustain. Chem. Eng. 5 (2017) 4249–4257, https://doi.org/10.1021/acssuschemeng.7b00242.
[35] S. Wang, B.Y. Guan, Y. Lu, X.W.D. Lou, Formation of hierarchical In_2S_3–$CdIn_2S_4$ heterostructured nanotubes for efficient and stable visible light CO_2 reduction, J. Am. Chem. Soc. 139 (2017) 17305–17308, https://doi.org/10.1021/jacs.7b10733.
[36] X. Chang, T. Wang, Z.-J. Zhao, P. Yang, J. Greeley, R. Mu, G. Zhang, Z. Gong, Z. Luo, J. Chen, Y. Cui, G.A. Ozin, J. Gong, Tuning Cu/Cu_2O interfaces for the reduction of carbon dioxide to methanol in aqueous solutions, Angew. Chem. Int. Ed. 57 (2018) 15415–15419, https://doi.org/10.1002/anie.201805256.
[37] Y. Xiao, C. Feng, J. Fu, F. Wang, C. Li, V.F. Kunzelmann, C.-M. Jiang, M. Nakabayashi, N. Shibata, I.D. Sharp, K. Domen, Y. Li, Band structure engineering and defect control of Ta_3N_5 for efficient photoelectrochemical water oxidation, Nat. Catal. 3 (2020) 932–940, https://doi.org/10.1038/s41929-020-00522-9.
[38] X. Chang, T. Wang, P. Yang, G. Zhang, J. Gong, The development of cocatalysts for photoelectrochemical CO_2 reduction, Adv. Mater. 31 (2019), 1804710, https://doi.org/10.1002/adma.201804710.
[39] S. Chen, J.J.M. Vequizo, Z. Pan, T. Hisatomi, M. Nakabayashi, L. Lin, Z. Wang, K. Kato, A. Yamakata, N. Shibata, T. Takata, T. Yamada, K. Domen, Surface modifications of $(ZnSe)_{0.5}(CuGa_{2.5}Se_{4.25})_{0.5}$ to promote photocatalytic Z-scheme overall water splitting, J. Am. Chem. Soc. 143 (2021) 10633–10641, https://doi.org/10.1021/jacs.1c03555.
[40] M.E. Aguirre, R. Zhou, A.J. Eugene, M.I. Guzman, M.A. Grela, Cu_2O/TiO_2 heterostructures for CO_2 reduction through a direct Z-scheme: protecting Cu_2O from photocorrosion, Appl. Catal. B Environ. 217 (2017) 485, https://doi.org/10.1016/j.apcatb.2017.05.058.
[41] K. Sun, M. Liu, J. Pei, D. Li, C. Ding, K. Wu, H.-L. Jiang, Incorporating transition-metal phosphides into metal-organic frameworks for enhanced photocatalysis, Angew. Chem. Int. Ed. 59 (2020) 22749–22755, https://doi.org/10.1002/anie.202011614.
[42] Y. Zhang, L.-Z. Dong, S. Li, X. Huang, J.-N. Chang, J.-H. Wang, J. Zhou, S.-L. Li, Y.-Q. Lan, Coordination environment dependent selectivity of single-site-Cu enriched crystalline porous catalysts in CO_2 reduction to CH_4, Nat. Commun. 12 (2021) 6390, https://doi.org/10.1038/s41467-021-26724-8.
[43] X. Zhou, J. Shan, L. Chen, B.Y. Xia, T. Ling, J. Duan, Y. Jiao, Y. Zheng, S.-Z. Qiao, Stabilizing Cu^{2+} ions by solid solutions to promote CO_2 electroreduction to methane, J. Am. Chem. Soc. 144 (2022) 2079–2084, https://doi.org/10.1021/jacs.1c12212.
[44] K.P. Kuhl, T. Hatsukade, E.R. Cave, D.N. Abram, J. Kibsgaard, T.F. Jaramillo, Electrocatalytic conversion of carbon dioxide to methane and methanol on transition metal surfaces, J. Am. Chem. Soc. 136 (2014) 14107–14113, https://doi.org/10.1021/ja505791r.
[45] Y. Wang, J. Zhao, Y. Li, C. Wang, Selective photocatalytic CO_2 reduction to CH_4 over Pt/In_2O_3: significant role of hydrogen adatom, Appl. Catal. B Environ. 226 (2018) 544, https://doi.org/10.1016/j.apcatb.2018.01.005.
[46] Y. Hori, A. Murata, R. Takahashi, Formation of hydrocarbons in the electrochemical reduction of carbon dioxide at a copper electrode in aqueous solution, J. Chem. Soc., Faraday Trans. 85 (1989) 2309–2326, https://doi.org/10.1039/F19898502309.
[47] W. Ma, S. Xie, X.-G. Zhang, F. Sun, J. Kang, Z. Jiang, Q. Zhang, D.-Y. Wu, Y. Wang, Promoting electrocatalytic CO_2 reduction to formate via sulfur-boosting water activation on indium surfaces, Nat. Commun. 10 (2019) 892, https://doi.org/10.1038/s41467-019-08805-x.
[48] X. Liu, P. Schlexer, J. Xiao, Y. Ji, L. Wang, R.B. Sandberg, M. Tang, K.S. Brown, H. Peng, S. Ringe, C. Hahn, T.F. Jaramillo, J.K. Nørskov, K. Chan, PH effects on the

electrochemical reduction of $CO_{(2)}$ towards C_2 products on stepped copper, Nat. Commun. 10 (2019) 32, https://doi.org/10.1038/s41467-018-07970-9.
[49] M. Ma, K. Djanashvili, W.A. Smith, Controllable hydrocarbon formation from the electrochemical reduction of CO_2 over Cu nanowire arrays, Angew. Chem. Int. Ed. 55 (2016) 6680–6684, https://doi.org/10.1002/anie.201601282.
[50] J. Resasco, Y. Lum, E. Clark, J.Z. Zeledon, A.T. Bell, Effects of anion Identity and concentration on electrochemical reduction of CO_2, ChemElectroChem 5 (2018) 1064–1072, https://doi.org/10.1002/celc.201701316.
[51] A.A. Peterson, F. Abild-Pedersen, F. Studt, J. Rossmeisl, J.K. Nørskov, How copper catalyzes the electroreduction of carbon dioxide into hydrocarbon fuels, Energy Environ. Sci. 3 (2010) 1311–1315, https://doi.org/10.1039/C0EE00071J.